JOURNAL OF GEOPHYSICAL RESEARCH, VOL. 113, A11302, doi:10.1029/2007JA012987, 2008

Anomalous enhancement of ionospheric electron content in the Asian-Australian region during a geomagnetically quiet day

B. Zhao,[1] W. Wan,[1] L. Liu,[1] K. Igarashi,[2] M. Nakamura,[2] L. J. Paxton,[3] S.-Y. Su,[4] G. Li,[1] and Z. Ren[1]

Received 11 December 2007; revised 20 June 2008; accepted 24 July 2008; published 1 November 2008.

[1] We investigate an event of anomalous enhancement in ionospheric electron content on 28 June 2002 from a network of 70 GPS receivers and a chain of ionosondes distributed around the Asian-Australian sector. After local sunset, the low-latitude peak electron density of the F_2 layer (N_mF_2) was observed to increase by 200% compared to the 27-day median value. Geomagnetic environment was quiet during 27–28 June as the SYM-H index was larger than −20 nT and *AE* was less than 200 nT under conditions of a constant northward interplanetary magnetic field *Bz*. A continuously enhanced eastward electric field has been identified as the main cause of this effect, though it is not fully consistent with the prediction of Scherliess and Fejer (1997) for wind disturbance dynamo model. Our observations show that the ionosphere was very disturbed in the Northern Hemisphere during summer even under low geomagnetic activity. The large ionospheric disturbance may be caused by the combination of the effects due to auroral activity and tides, a combination that still needs further investigation. This work suggests that studying very large day-to-day variability under quiet geomagnetic conditions could reveal more about the coupling processes between the ionosphere and lower atmosphere.

Citation: Zhao, B., W. Wan, L. Liu, K. Igarashi, M. Nakamura, L. J. Paxton, S.-Y. Su, G. Li, and Z. Ren (2008), Anomalous enhancement of ionospheric electron content in the Asian-Australian region during a geomagnetically quiet day, *J. Geophys. Res.*, *113*, A11302, doi:10.1029/2007JA012987.

1. Introduction

[2] It is well known that ionospheric F_2-layer parameters have a large day-to-day variability. The peak electron density (N_mF_2) of the ionosphere varies from day to day with a standard deviation of typically about 20% by day and 33% by night [*Rishbeth and Mendillo*, 2001]. Since the day-to-day variability is of great importance to the development of empirical models such as the International Reference Ionosphere [*Bilitza*, 2001], extensive studies have been made to reveal the dependence of the ionosphere on local time, seasonal and solar activity in different regions [e.g., *Forbes et al.*, 2000; *Kouris and Fotiadis*, 2002; *Ezquer et al.*, 2004; *Zhang et al.*, 2004; *Dabas et al.*, 2006]. As discussed by *Forbes et al.* [2000] and *Fuller-Rowell et al.* [2000], the day-to-day variability, which is greater in the region of the equatorial ionization anomaly (EIA) area and at high latitudes, is attributed to "solar," "geomagnetic," and "other" causes. The "other" influences, which seem to be originated from lower part of the atmosphere, were termed "meteorological" by *Rishbeth and Mendillo* [2001]. Generally, these papers broadly agree with that a large part of this variability is attributed to the geomagnetic activity, although meteorological effects may make a comparable contribution. However, there is a large class of disturbances that are not directly due to geomagnetic activity but have their origin in the atmosphere itself [e.g., *Blagoveshchensky et al.*, 2006; *Laštovička and Šauli*, 1999; *Mikhailov et al.*, 2004, 2007a, 2007b]. A number of studies have shown that meteorological processes such as planetary waves, gravity waves, and tides can have direct or indirect effects on the *F* region ionosphere [*Laštovička*, 2006; *Rishbeth*, 2006]. Planetary waves of large spatial extent and long period are more promising as a cause of *F*-layer variations. The reviews by *Kazimirovsky et al.* [2003] and *Altadill et al.* [2004] cited many papers dealing with planetary wave effects, both in the F_2 layer and lower heights. On the basis of spectral analysis, wave structures with periods of about 2–16 days in the *F* region parameters are clearly detected [*Altadill and Apostolov*, 2003]. The problem is that ionospheric disturbances caused by magnetic storms usually last 1–3 days or longer depending on

[1]Beijing National Observatory of Space Environment, Institute of Geology and Geophysics, Chinese Academy of Sciences, Beijing, China.
[2]National Institute of Information and Communications Technology, Tokyo, Japan.
[3]Johns Hopkins University Applied Physics Laboratory, Laurel, Maryland, USA.
[4]Institute of Space Science and Center for Space and Remote Sensing Research, National Central University, Chung-li, Taiwan.

0148-0227/08/2007JA012987$09.00

the intensity of the solar wind energy input and global thermospheric conditions [*Field et al.*, 1998; *Scherliess and Fejer*, 1997; *Huang et al.*, 2005; *Mendillo*, 2006]. Besides, the ionosphere, especially in the EIA region, not only responds to magnetic storms but also is affected by the electrodynamic coupling between the magnetosphere and ionosphere known as the penetration electric field effect [e.g., *Fejer and Scherliess*, 1995]. Hence, it is difficult to separate the effects of geomagnetic activity and meteorological influence, especially during the solar maximum period when geomagnetic disturbance are common and they occur at a high enough rate that one is justified in asking whether the upper atmosphere has returned to its quiescent state.

[3] *Mikhailov et al.* [2004] put forward a term "Q disturbances" referring to hourly ($N_mF_2/N_mF_{2\mathrm{med}} - 1$) deviations of more than 40% if all 3-h *Ap* indices being ≤ 7 for 24 previous hours. This paper and a later work by *Depueva et al.* [2005] described the morphology pattern of Q disturbances under different local time, season, and geographic location conditions using observations from 26 ionosonde stations in the Northern Hemisphere and 2 around the geomagnetic equator. Later, an interpretation of some of the features was provided by *Mikhailov et al.* [2007a, 2007b] based on Millstone Hill incoherent scatter radar (ISR). *Goncharenko et al.* [2006] also revealed a pronounced negative Q-disturbance effect using the Millstone Hill ISR and TIMED/GUVI observations and attributed it to the IMF *By* variations.

[4] Another quiet time disturbance is termed the prestorm enhancement by *Burešová and Laštovička* [2007] or a positive phase before the beginning of a geomagnetic storm by *Danilov* [2001] and *Kane* [1973]. Typical examples of the prestorm enhancement in the maximum electron density (N_mF_2) or the critical frequency (f_oF_2) can be found at Chilton (358.7°E, 51.6°N) on 28 October 2003 [*Burešová and Laštovička*, 2007] and at Murmansk on 1 March 1981 [*Danilov*, 2001]. In contrast to these studies which focus on the middle and high latitudes, *Liu et al.* [2008] found strong prestorm enhancements in the EIA region which were associated with an enhanced equatorial eastward zonal electric field. Their results indicate that the prestorm enhancements are not accompanied by a corresponding change of ionospheric peak height (h_mF_2). This h_mF_2 behavior during prestorm enhancements may be explained in terms of the coupling nature of parallel and perpendicular dynamics at low latitudes [e.g., *Behnke and Harper*, 1973; *Rishbeth et al.*, 1978].

[5] Abnormal changes in the ionospheric parameters under quiet geomagnetic conditions over an equatorial station Kodaikanal (10.23°N, 77.48°E, Dip: 3.5°N) was reported by *Sastri* [1998]. Large, sudden increases of 52–117 km in the height of the bottom-side *F* layer ($h'F$), were observed in the postsunset sector (1800–2000 LT) on eight geomagnetically quiet days ($Ap \leq 5$) during 1957–1969. The perturbations were characterized by postnoon enhancements of the equatorial electrojet (EEJ) and an attendant intensification of the EIA before evening. Recently, by using total electron content (TEC) values derived from GPS signals over Japan, *Kutiev et al.* [2006, 2007] analyzed the appearance and development of enhancements of TEC of equatorial origin (ETEs); a part of the EIA, occurring outside initial and main phases of geomagnetic storms. They found that ETE structures appear mainly as single-crest structures in the local evening hours with a TEC peak around 1900 LT. They also observed that most of the ETE events appeared during periods of low geomagnetic activity in the 1–3 days after the main phase of the storms. Their work provides a clue in clarifying the sources of ionospheric variability through the investigation of large ionospheric disturbances under geomagnetically quiet conditions.

[6] In the present study, we report an abnormal behavior of ionospheric F_2 layer in the east Asian region where N_mF_2 at the EIA northern crest increased more than 200% compared to the 27-day median value for times after 1800 LT during a geomagnetically quiet period. By using GPS TEC and a chain of ionosondes in the Asian-Australian sector, a continuously enhanced fountain effect has been identified to be the main cause of this effect. Our study suggests that this extremely large day-to-day variability or so-called Q disturbance is caused by the combination of auroral activity and a disturbance originated in the lower atmosphere.

2. Data Sets

[7] The GPS data are from the Crust Movement Observation Network of China (CMONOC) and the International Global Navigation Satellite System Service (IGS) GPS tracking network covering the Asian-Australian sector. Around 70 GPS receivers were used to derive the grid TEC value at longitudes 120°–140°E. Using a least squares fit and nearest neighbor interpolation method, slant TEC observations are converted to vertical TEC data on a 2.5° grid. The details of the algorithm used are described elsewhere [*Zhao et al.*, 2005].

[8] The ionosonde data used for the present study are provided by the Institute of Geology and Geophysics of the Chinese Academy of Sciences, websites of the National Institute of Information and Communications Technology of Japan and the Ionospheric Prediction Service of Australia. The ionosonde stations are Wakkanai (45.4°N, 141.7°E; 40.5°N magnetic latitude), Kokubunji (35.7°N, 139.5°E; 30.0°N), Wuhan (30.6°N, 114.4°E; 26.7°N), Yamagawa (31.2°N, 130.6°E; 26.1°N), Okinawa (26.7°N, 128.2°E; 21.2°N), Darwin (12.5°S, 130.9°E; 23.5 °S), and Townsville (19.6°S, 146.9°E; 30.4°S). Ionograms of Chinese and Japanese ionosondes were obtained every quarter hour. Ionograms for Australian ionosondes were obtained every hour and were interpolated to every quarter hour for comparison. All the ionograms were scaled manually. The SAO-Explorer software (available at http://ulcar.uml.edu/downloads.html) was used to obtain the basic ionospheric parameters for the Chinese ionosonde [*Reinisch et al.*, 2005]. For Japanese ionosonde data, we downloaded the images of the ionograms in PNG format from NICT and developed our own software to extract the O wave trace. We then used the true height inversion program NHPC [*Huang and Reinisch*, 2001] to obtain the ionospheric height profile information.

[9] Global Ionospheric Maps (GIMs) of TEC were provided from NASA Jet Propulsion Laboratory. There is a rich literature describing the development of JPL GIM [e.g.,

Mannucci et al., 1998], as well as their use in studies of ionospheric behavior, particularly under disturbed conditions [*Ho et al.*, 1998]. The GPS system and the JPL GIMs have become a standard ionospheric diagnostic tool. At the same time, the ROCSAT-1 satellite made several passes over Asian-Australian sector when a severe plasma enhancement was observed in the evening. Plasma drift data obtained by the ROCSAT-1 satellite were used to interpret the regional characteristics of the event when a large electron enhancement was observed on 28 June. To discuss changes in the thermospheric composition, we use experimental data of the daytime O/N_2 column density obtained by the Global Ultraviolet Imager (GUVI) instrument on board the TIMED satellite. The GUVI column O/N_2 ratio is determined from the O (135.6 nm) and N_2 (LBH) emissions [*Christensen et al.*, 2003; *Paxton et al.*, 2004; *Strickland et al.*, 2004] and is estimated with $1.75^\circ \times 1.75^\circ$ spatial resolution. Detailed discussions on the definition of O/N_2 column density ratio and the analysis technique can be found in the above-referenced papers and references therein.

[10] The level of geomagnetic activity during the examined period is indicated by the *Kp*, SYM-H, *AE*, and Hpi (hemispheric power index issued by the NOAA Space Environment Center) indices. *AE* and Hpi are used as an indicator of substorm activity. The *Kp* index describes geomagnetic conditions at midlatitudes, and the SYM-H index describes geomagnetic conditions at low latitudes. The SYM-H index is used as a surrogate for a higher-resolution *Dst* index. It also should be mentioned that the *AE* index downloaded from the WDC-Kyoto Web site is provisional data. Solar wind interplanetary magnetic field (IMF) *By* and *Bz* components in the GSM coordinate are obtained from the ACE satellite and to compute the dawn-dusk component of interplanetary electric field *Ey* (Ey [mV/m] = $-$Bz [nT] $\times$ Vx [km/s] $\times$ 10^{-3}, Vx being the solar wind velocity in Sun-Earth direction) and solar wind dynamic pressure P_{dyn} (P_{dyn} [nPa] = $m_H \times n$ [cm^{-3}] $\times$ V^2 [km/s]; *n* being the proton number density, and V being the bulk speed). We also use P_{dyn} from the Near-Earth Heliospheric data set (OMNI) database to compensate for the data gaps in the ACE satellite.

3. Results

3.1. Geomagnetic Environment and Associated TEC Variation

[11] Figures 1a and 1b show the contour maps of the TEC and ΔTEC (where ΔTEC is the difference between the TEC and the 27-day smooth median value) as a function of universal time and latitude for 26–29 June 2002. Figure 1c plots the SYM-H, *AE*, Hpi, and 3-h *Kp* indices during the corresponding period. Figures 1d–1f show the development of IMF *Bz*, dawn-to-dusk component of the interplanetary electric field *Ey*, IMF *By* component, and solar wind dynamic pressure P_{dyn}. As shown in Figure 1, SYM-H remained fairly small during this period. It decreased to -20, -19, and -18 nT at 0000 UT and 1800 UT on 26 June and 1800 UT on 27 June, respectively. According to the magnetic storm classification of *Gonzalez et al.* [1994], these disturbances are too small to be regarded as a storm. The maximum *Kp* is 2.7 on 26 June and 1 on 27 and 28 June. Corresponding to the decrease in SYM-H index, some small auroral activities occurred as *AE* increased to 300 and 450 nT at 0000 UT and 1800 UT on 26 June and remained very low on 27 June. Hpi increased to 35, 48, and 23 GW during the three SYM-H depressions. On 26 June, the IMF *Bz* component turned southward from 1200 to 2200 UT and was associated with enhancement of auroral activity. *Bz* was generally positive after 2000 UT on 28 June. IMF *By* index kept positive with a magnitude of 3 nT until 1800 UT on 28 June. The geomagnetic environment on 28 June was rather quiet as SYM-H varied from 0$\sim$5 nT and *AE* and Hpi were quite low. However, there was a large enhancement in TEC observed in the EIA region on this day as illustrated in Figures 1a and 1b. For most of the time during 27–28 June, *Ey* is low as is P_{dyn}, which avoids the situation described by *Huang et al.* [2002] wherein the solar wind dynamic pressure causes global magnetosphere and ionosphere disturbances. The phase difference between values from ACE and OMNI database may be due to different data source when calculating P_{dyn}. There is a data gap in the P_{dyn} data after 1200 UT on 28 June. In the northern crest EIA, enhancement of ΔTEC started around 0845 UT while in the southern crest about 0600 UT. Furthermore, solar flux *F*10.7 index during the period changed little. We also checked the SOHO/SEM EUV fluxes and found no solar flare event during this period.

3.2. Ionosonde Observations in the Asian-Australian Region

[12] Figure 2 shows the evolution of N_mF_2 in the Asian-Australian ionosonde chain during 26–29 June. The gray line represents the 27-day smooth median value. A significant increase in N_mF_2, which began at around 0845 UT on 28 June, was seen at the low-latitude station Okinawa. In the postsunset sector, N_mF_2 increased from 0.9×10^6cm^{-3} to 2.8×10^6cm^{-3} (8.5 MHz to 15.5 MHz for f_oF_2), about 200% of the median value. A similar enhancement in N_mF_2 was also observed at Darwin in the Southern Hemisphere but started 2 h earlier in consistence with the interpolations in the ΔTEC contour map. Actually, before 0600 UT on the 28 June there was a small enhancement in N_mF_2 at Darwin. Note that in Figure 1 there was also a weak increase observed in TEC around 0300–0500 UT at 10°S. At Kokubunji and Wuhan, the postsunset N_mF_2 increment occurred at 1045 UT, 2 h delay with respect to the enhancement of N_mF_2 at Okinawa, indicating an expansion process of EIA. Figure 3 presents the time evolution of h_mF_2 during 27–29 June. As seen in h_mF_2 for stations Kokubunji, Wuhan and Okinawa, there were usually valleys around 1000 UT for reference values denoted by the gray line. However, a maximum increase of about 50 km appeared on 28 June during 0800–1200 UT. Here the reference value is the average of 26, 27, and 29 June. At this time, TEC in Figure 1 shows depletion at magnetic equatorial area and large increase at crest region suggesting there was enhanced fountain effect during the period. Near-simultaneous elevation of *F* layer at low latitude and enhanced fountain effect of EIA both indicate there was most possibly an extra eastward electric field impinging on the equatorial ionosphere during 0800–1200 UT. However, at the middle-latitude station Wakkanai, h_mF_2 showed an initial decrease at 0800–1000 UT on 28 June. We will give a possible explanation for this in section 3.3.

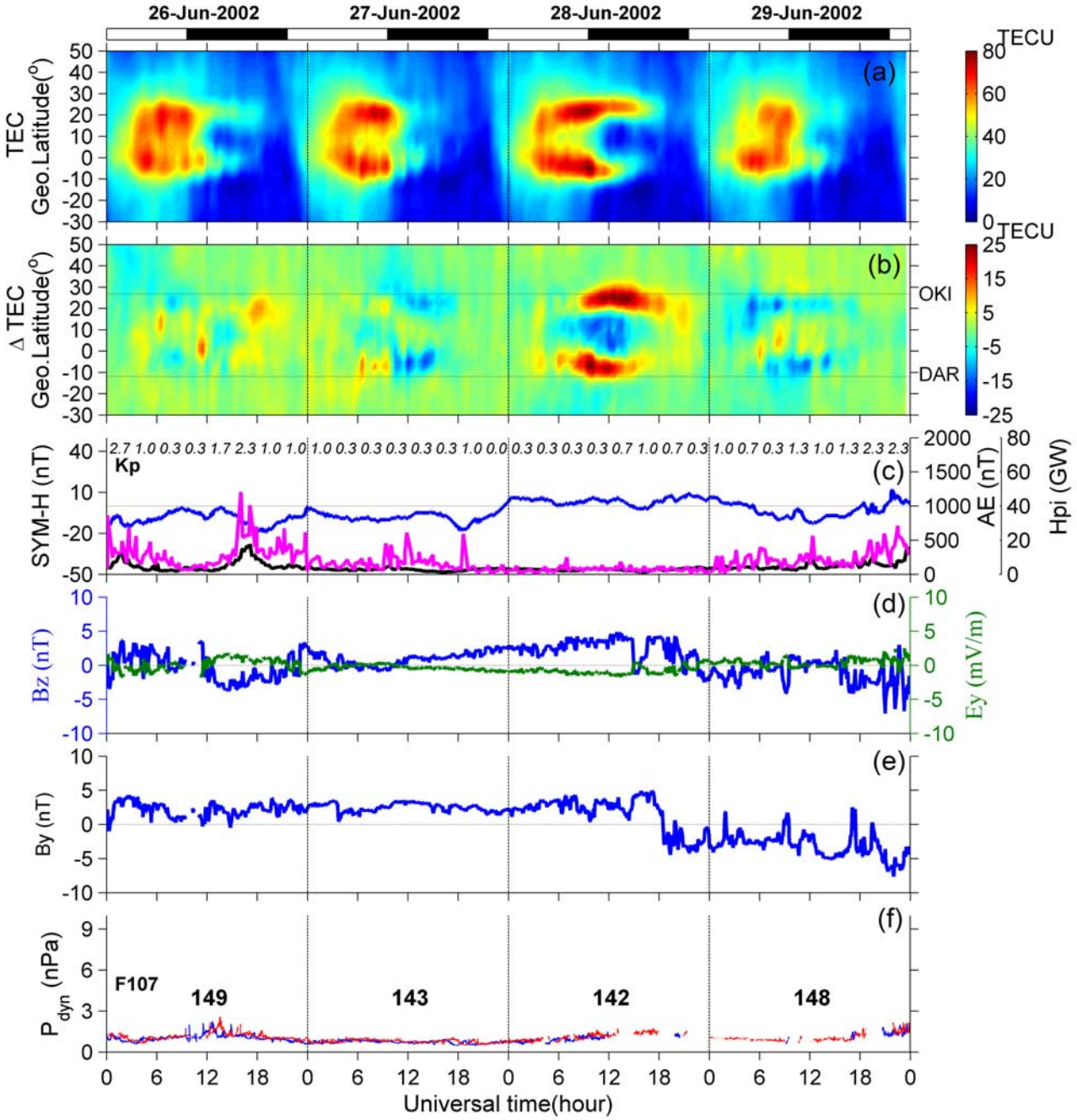

Figure 1. (a, b) Total electron content (TEC) and the deviations of TEC (dTEC) from the median value along 110°E longitude during 26–29 June 2002; (c) SYM-H (blue line), *AE* (black line), hemispheric power index (Hpi, magenta line), and 3-hourly *Kp* (text); (d) interplanetary magnetic field (IMF) *Bz* (blue line) and *Ey* (green line); (e) IMF *By*; and (f) solar wind dynamic pressure P_{dyn} from ACE (blue line) and Near-Earth Heliospheric data set (OMNI) (red line) and solar flux *F*10.7 index (text). Here and in Figures 2 and 3 the horizontal bar at the top indicates the daytime (white) and nighttime (black). OKI, Okinawa; DAR, Darwin.

[13] Note that actually before the appearance of significant enhancement at Okinawa, the N_mF_2 increase already emerged at Wakkanai and Kokubunji around 2000 UT on 27 June and lasted until 1000 UT on 28 June. This positive phase from predawn sector to the afternoon sector was not seen evidently in TEC data shown in Figures 1a and 1b. The increase in TEC was not as significant as that in N_mF_2. The increased N_mF_2 and nearly unchanged TEC suggest that the *F* layer was compressed with reduced scale height in the topside ionosphere. This condition may possibly result from the vertical meridional wind shear as pointed out by *Lu et al.* [2001], which shows that when the meridional wind is the dominant influence on h_mF_2 and f_oF_2, the positive/negative vertical wind shear due to the upward propagation

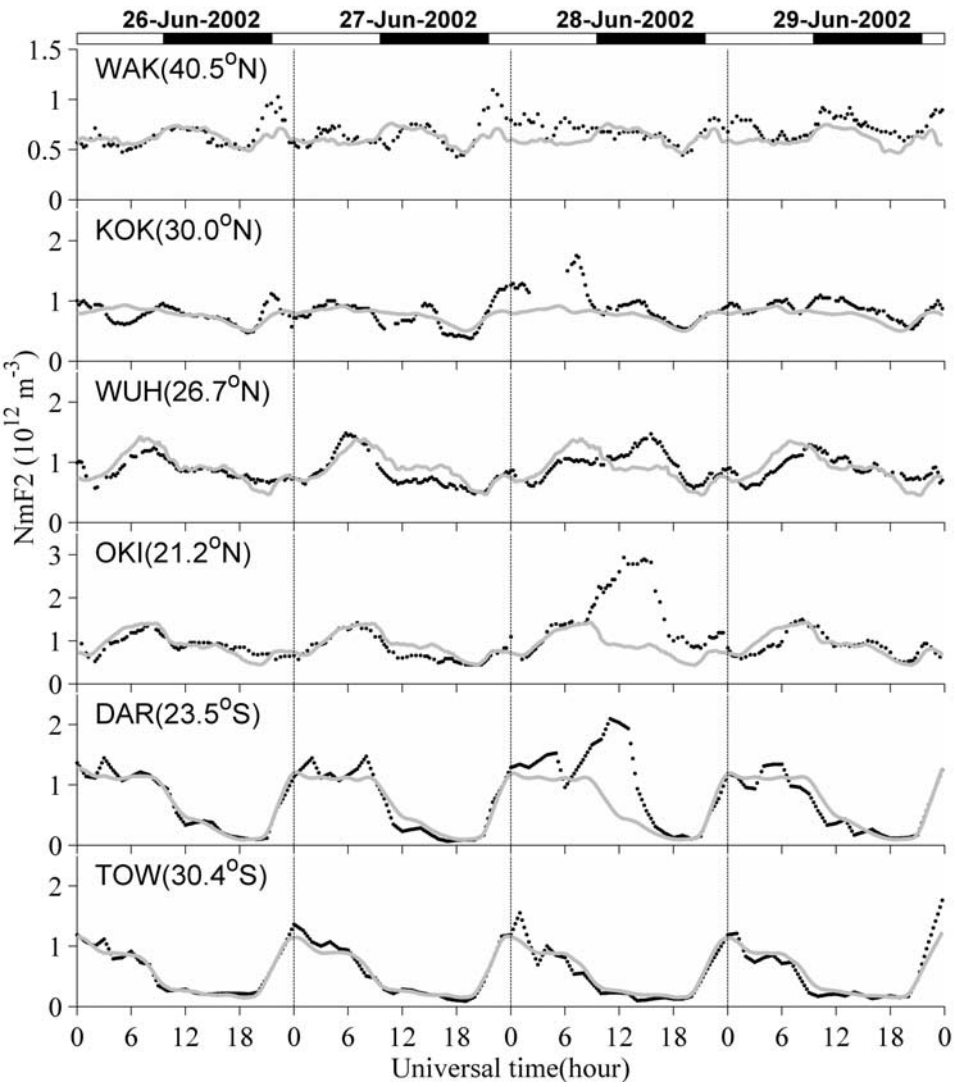

Figure 2. From top to bottom are N_mF_2 at ionosondes Wakkanai (WAK), Kukubunji (KOK), Wuhan (WUH), Okinawa (OKI), Darwin (DAR), and Townsville (TOW) during 26–29 June. Gray lines indicate the 27-day median. The magnetic latitude of each station is shown in parentheses.

gravity waves can compress/expand the layer, leading to the anticorrelation between the h_mF_2 and f_oF_2. These gravity waves may originate from the auroral oval or generated by the localized sources in the lower atmosphere. The data gap at Kokubunji around 0300–0600 UT on 28 June is due to the formation of an extraordinary strong sporadic E (E_s) layer which blotted out the F_2-layer trace. Enhanced h_mF_2 was seen to occur earlier, at 1200 UT, on 27 June and fluctuated during 1800–2400 UT. The irregular h_mF_2 during this period was due to the spread F and a strong E_s layer. Thus, the positive ionospheric disturbances after 1800 UT on the 27 June (Figure 2) at middle-latitude stations Wakkanai and Kokubunji were most probably a response to the weak depression of SYM-H together with the peak in Hpi observed at the 1200–1800 UT. Contrary to what is observed at Kokubunji at around 0600 UT on 28 June, N_mF_2 of the Wuhan station shows an evident decrease. As pointed out by *Burge et al.* [1973], equatorward directed winds will oppose the poleward transport of ionization along the magnetic fields. This will hinder the formation of the equatorial anomaly and generate negative storm effects in the anomaly crest regions and positive storm effects near the equator. Model calculations by *Rüster and King* [1976] confirmed the validity of this concept. They noted that without the fountain effect, equatorward directed winds will increase the ionization density, just as the case at middle latitudes. This tendency prevails down to about 20° magnetic latitudes where a changeover takes place.

[14] Figure 4 shows the f_oE_s variation at Kokubunji, Wuhan, Yamagawa, and Okinawa from 1500 UT 23 June to 1500 UT 29 June. The top axis shows the local time from 24 to 29 June. An abnormally large enhancement of f_oE_s was observed at Kokubunji, Yamagawa, and Okinawa at 0700–0900 UT, 0–3 h before the start of the postsunset anomalous enhancement, which is denoted as a vertical dashed line on 28 June. Besides, before 0300 UT, at Okinawa, f_oE_s was also strong leading to the appearance of an intensified semidiurnal variation. Furthermore, f_oE_s at

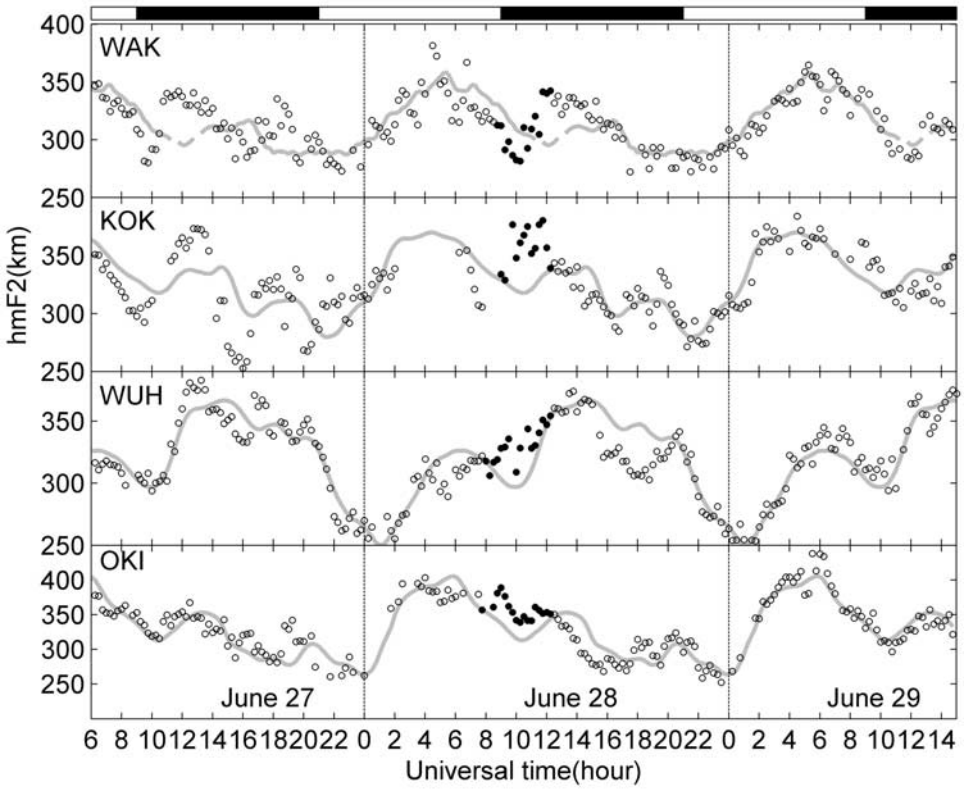

Figure 3. From top to bottom are h_mF_2 (open circles) at the ionosondes at Wakkanai, Kukubunji, Wuhan, and Okinawa during 27–29 June 2002. It is shown that simultaneous increases in h_mF_2 (solid circles) were observed at 0800–1200 UT on 28 June at Kokubunji, Wuhan, and Okinawa. The gray line in each case represents the reference value.

nearly all the stations was generally seen to be higher on local 26 and 28 June but lower on 25 and 27 June. These features maybe associated with processes originating in the lower atmosphere: a question that needs a further study.

3.3. Combined Observations From ROCSAT-1 and GIM TEC

[15] Figure 5 illustrates the comparison of JPL GIM TEC difference maps (the 27-day median has been subtracted

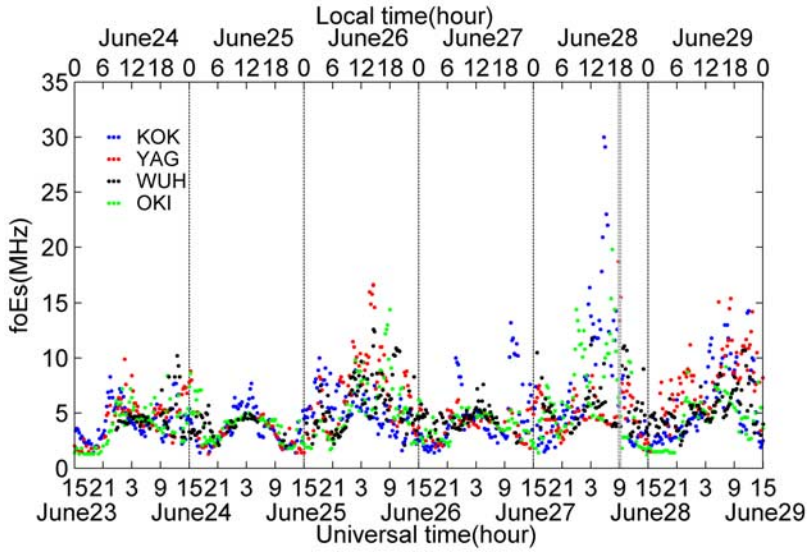

Figure 4. Evolution of sporadic E critical frequencies (f_oE_s) during 23–29 June at Kokubunji (blue circles), Yamagawa (red circles), Wuhan (black circles), and Okinawa (green circles). The vertical gray dashed line at 0900 UT on 27 June denotes the time at which extreme enhancement started.

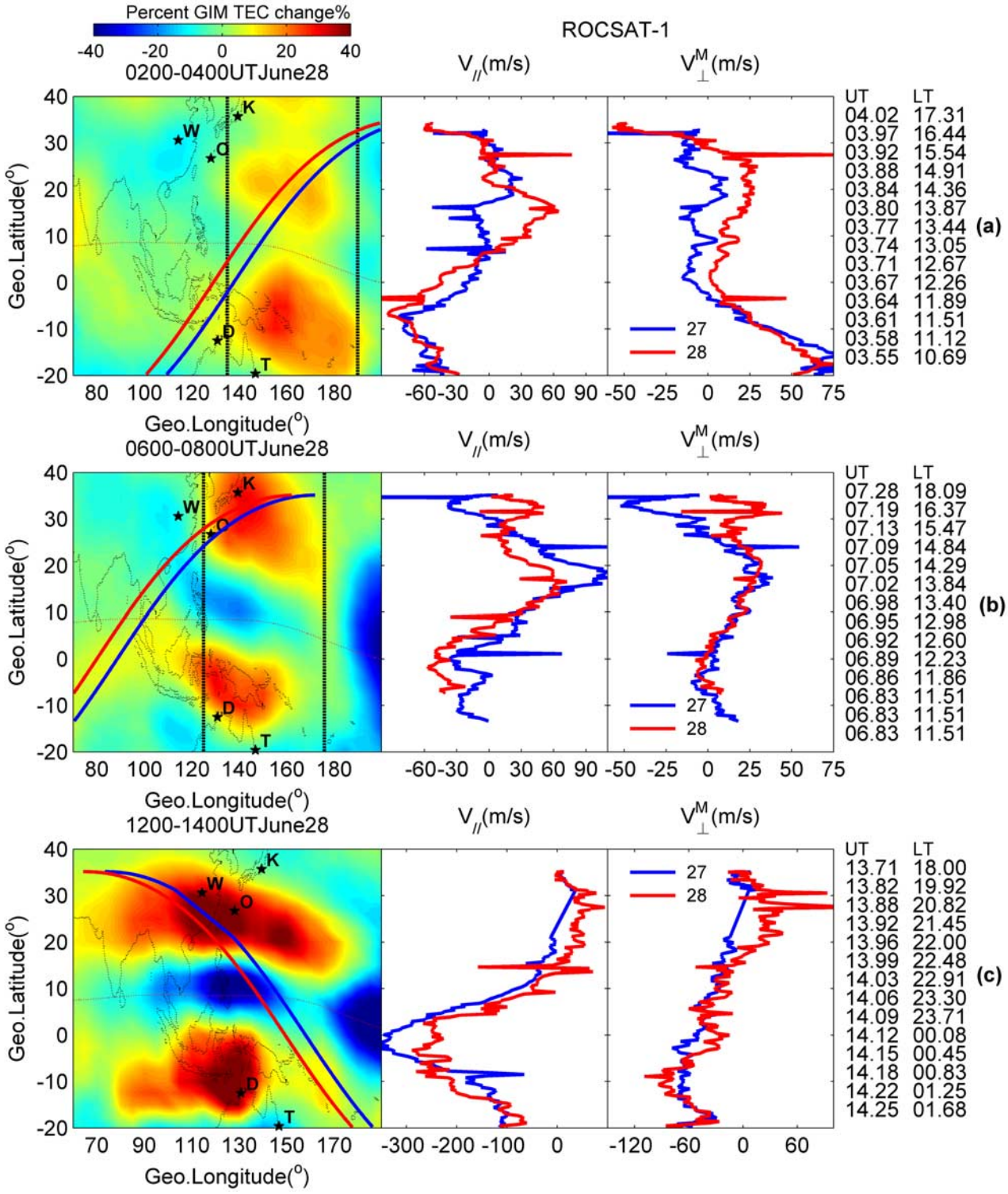

Figure 5. Comparison of global TEC difference maps with in situ drift measurements from ROCSAT-1. The left maps show the TEC at (a) 0200–0400 UT on 28 June and the ground tracks of ROCSAT-1 crossing the area during the period on 28 June (red line) and 27 June (blue line), (b) 0600–0800 UT on 28 June, and (c) 1200–1400 UT on 28 June. The black stars on the maps indicate ionosonde stations marked with the first letter of their name; for example, "O" denotes Okinawa. The thin dashed lines indicate the location dip equator. The profiles on the right show the drift measurements along the ROCSAT-1 track. $V_{//}$ is the parallel-to-field component of ion drift velocity: a positive value is northward. $V_{\perp}^{M}$ is the component of ion drift velocity in the magnetic meridian plane perpendicular to the vector field: a positive value is outward.

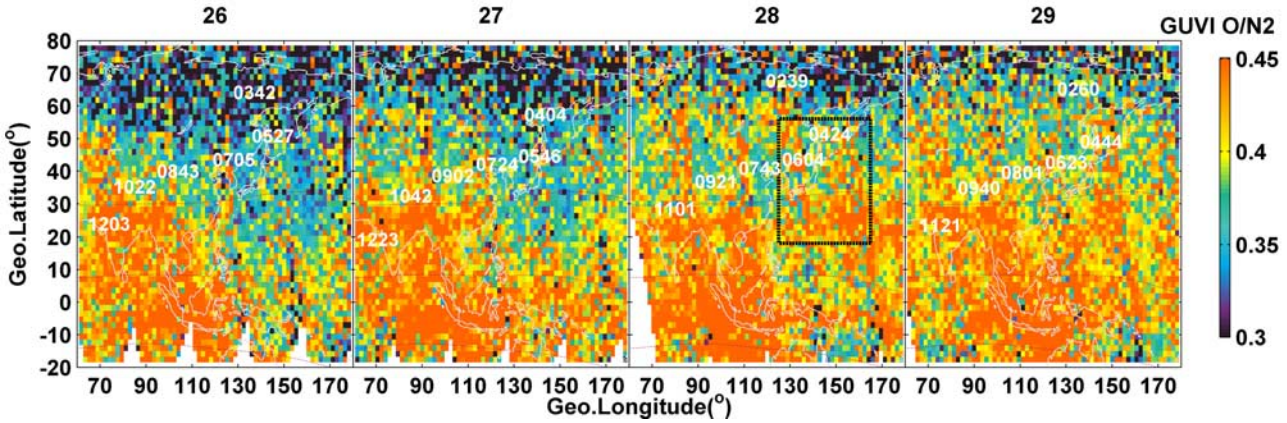

Figure 6. Global Ultraviolet Imager (GUVI) O/N_2 ratio during 26–29 June 2002. The data were recorded around 1530 LT for the longitudes 70°–170°E. The centered universal time, mean value of each orbit is labeled as white text. After 27 June, an increase in O/N_2 can be seen over the east Asian region as denoted inside the rectangle. The thin dashed lines represent the dip inclinations of 0° and ±30°.

from the daily value at each time interval) for the Western Pacific area with in situ drift measurements from ROCSAT-1, ~600 km in altitude. The TEC map in Figure 5a shows that the enhanced fountain effect started at 0200–0400 UT on 28 June over a limited longitude range (about 130–190°E as indicated by dashed lines). The ROCSAT-1 satellite just passed through the area at 0400 UT. The red line in Figure 5a denotes the value on 28 June, and the blue line denotes the value on 27 June. The profiles on the right show the drifts of the corresponding tracks. The $V_{//}$ is the parallel-to-field component of the ion drift velocity; the positive values represent the northward plasma flows. The $V_{\perp}^{M}$ represents the ion drift component in the magnetic meridian plane, which is perpendicular to the geomagnetic field; the positive values correspond to outward plasma flows [*Su et al.*, 2002]. It can be seen that inside the enhanced EIA region, $V_{\perp}^{M}$ shows a 30 m/s increase in the outward direction comparing to the value of the previous day indicating an extra eastward electric field. From 10 to 20°N, inside the crest region, $V_{//}$ shows a maximum increase of 60 m/s whereas from 10°N–10°S there is a 20 m/s decrease indicating that the enhanced fountain effect has resulted in a larger plasma diffusion. The local time of the enhanced EIA region covers around 1200–1630 LT.

[16] Figure 5b shows that at 0720 UT on 28 June, inside the enhanced northern crest region, $V_{//}$ and $V_{\perp}^{M}$ increased by 60 m/s and 75 m/s, respectively, compared to the values of 27 June. We believe this to be caused by a more intensified eastward electric field compared to the values of Figure 5a. Note that in Figure 3, the h_mF_2 at the low-latitude stations Okinawa and Wuhan showed increases at 0800–1000 UT on 28 June while at the higher-latitude station at Wakkanai a decrease was observed. Such h_mF_2 behaviors may be possibly explained in terms of the coupling nature of parallel and perpendicular dynamics at middle latitudes [e.g., *Behnke and Harper*, 1973; *Rishbeth et al.*, 1978]. A stronger eastward electric field produces larger field-aligned ion flows, which tends to cancel out the possible lifting of the peak height of the F_2 layer at middle-low latitudes due to that eastward electric field. This may result in nearly horizontal motion or even a decrease of the height of the F layer as observed at larger magnetic inclination stations such as Wakkanai. In Figure 5b between 100 and 120°E and 15–28°N, the area below Wuhan (W), $V_{//}$ showed a general decrease of 30 m/s, suggesting that plasma diffusing is being retarded by an enhanced equatorward meridional wind. This enhanced equatorward wind resulted in the depletion near the crest region that was observed in N_mF_2 at Wuhan during this period. The local time of the enhanced EIA region covers around 1500–1800 LT.

[17] Another feature consistent with the ionosonde observations is that the southern enhanced EIA is not always symmetric with its northern partner. Note that the location of southern EIA is close to the longitudes 160–200°E, which has a 10° positive magnetic declination. The diffusion velocity has a westward component in the Southern Hemisphere making the positive phase shift several degrees to the west. Thus, at Darwin (denoted by D in Figure 5b), the ionospheric parameters presented positive phase earlier than what was observed at Okinawa (O). Figure 5c illustrates the extraordinarily intensified EIA at 1200–1400 UT on 28 June. $V_{\perp}^{M}$ shows about a 50 m/s increase in the northern enhanced EIA area. Note that two large spikes in $V_{\perp}^{M}$ were observed: they could be the signature of plasma bubbles. The local time of enhanced EIA during this time covers from 1800 to 2400 LT which is consistent with this suggestion.

3.4. Disturbance in Thermospheric Composition

[18] Figure 6 presents the GUVI O/N_2 distribution during 26–29 June in the Asian region. The mean universal time of every orbit was labeled on the map. The estimated errors in O/N_2 might reach 10% for high O/N_2 values at latitudes above 60° but are expected to be close to 5% for low O/N_2 values and at lower latitudes [*Christensen et al.*, 2003; *Strickland et al.*, 2004]. The TIMED spacecraft has an inclination of 74.1° with a 97.8 min orbital period. The orbital precession rate is such that the beta angle (the angle between the Earth-Sun vector and the orbital plane) passes through zero every 120 days; the local time of the ascending node of the orbit varies with this periodicity. As a consequence, GUVI samples all local solar times every 60 days,

counting both the ascending and descending node orbits. The local time of the ascending node changes by just 12 min per day. As shown in Figure 6, the area inside the dashed rectangle on 28 June denoted the east Asian region where the satellite crossed the equator on the dayside close to ~1530 LT during this period. Generally, O/N_2 in this area was 0.45 on 28 and 29 June, which is about 30% larger than 0.35 on 26 and 27 June. This enhancement though not large may favor the maintenance of the enhanced plasma density in the east Asian area as observed in TEC and N_mF_2.

4. Discussion

[19] We have shown, from ground- and space-based instruments, even under geomagnetically quiet conditions, the ionosphere can undergo significant changes in the east Asian region. The main features of this event can be summarized as follows: (1) Anomalous enhancements in N_mF_2 and TEC at low latitudes are preceded by 24 h of geomagnetically quiet conditions and low auroral activity (*AE* was around 500 nT, SYM-H > −30 nT) for the two previous days. These conditions are similar to the events of 25 March 2004 investigated by *Kutiev et al.* [2007]. (2) These anomalous low-latitude enhancements tend to occur with peaks around latitudes of the EIA crests. (3) The anomalous enhancements exhibited a local time dependence, which evolved from noon to postsunset and became much intensified in the postsunset sector. (4) Positive storm effects in N_mF_2 associated with height disturbances were observed at middle- to low-latitude stations before they were observed at lower latitudes. (5) The E_s layer experienced a great increase before the start of the anomalous enhancements in the east Asian region. These features could be clearly identified in Figures 1–4. GIM TEC and drift measurements from the ROCSAT-1 satellite showed that the anomalous enhancement was caused by an enhanced eastward electric field as shown in Figure 5. This interpretation is also supported by the simultaneously observation, at low-latitude stations, of increased h_mF_2 values.

[20] A large ionospheric disturbance at middle latitudes under low geomagnetic activity conditions has been investigated by *Goncharenko et al.* [2006]. In their case, a minor storm occurred from 1200 UT of 15 April 2002 to 0700 UT of 16 April, which is indicated with SYM-H index larger than −25 nT and Hpi less than 25 GW. The IMF *Bz* remained generally southward during the period. The most interesting finding of that study was that a large negative ionospheric storm effect was observed in middle latitude of American region when there was a strong positive IMF *By* component. *Goncharenko et al.* [2006] attribute the effect to the changes in the plasma convection pattern at high latitudes due to a positive IMF *By*. Through the modification of high-latitude wind fields, decreased O/N_2 has been transported by the enhanced meridional wind to lower latitudes as observed by GUVI satellite. However, our case is different from theirs as the IMF *Bz* remained always northward, which should lessen the high-latitude convection effect. The feature of interest is that GUVI O/N_2 shows an increase around 1500 LT after 27 June 2002 in the east Asian region. Model simulations showed that the divergence and upwelling of the polar upper atmosphere during a storm could set up a Hadley-type circulation cell that produces convergence and downwelling in the low and middle latitudes [*Rishbeth et al.*, 1987; *Burns et al.*, 1995]. The downwelling of the atmosphere causes a decrease in molecular gases in the *F* region and induces a positive storm effect. Thermospheric neutral composition change is an alternative explanation for positive ionospheric storm effect. This effect requires further observational evidence for its validation. The key point is: Do low values of geomagnetic indices really mean that it will be a geomagnetically quiet day? As shown in Figures 2 and 3, positive storm effects after 1800 UT on 27 June at Wakkanai and Kokubunji could be caused by enhanced meridional winds. The heating of high-latitude region launches equatorward wind surges that drag the low- to middle-latitude plasma to higher altitudes along the magnetic field lines. An uplift of the plasma in that region induces an increase in plasma density owing to the decrease in O^+ loss rate at higher altitudes [*Prölss*, 1993]. *Prölss* [1993] used the *AE* index as a reference for substorm onset and observed an increase in h_mF_2 and N_mF_2, with a few hours delay (a 1–2 h delay at middle latitudes and 3–5 h delay at low latitudes), after substorm onset. For the present case, shown in Figure 1, the *AE* index on 27 June is too small, and IMF *Bz* was northward. However, an impulsive value of the Hpi index of 20 GW appeared on that day. Furthermore, on 26 June, there was substorm event where *AE* increased to 450 nT and Hpi to 48 GW around 1600 UT. These may have produced a combined effect that led to a relatively strong equatorward wind disturbance. This wind disturbance was superimposed on the normal summer to winter circulation and may have caused a large ionospheric storm effect though there was no magnetic storm event visible in SYM-H data.

[21] At low latitudes, the anomalous intensification of the EIA should be caused by the external electric field. We have ruled out the possibility of the penetration electric fields as the interplanetary conditions were stable. For the present case, we tend to believe that the anomalous enhancement of electron content in the east Asian–Australian region is unlikely to be caused solely by the substorm occurred on 26 June since (1) the wind disturbance dynamo effect occurs within 22–28 h after large increases in the high-latitude currents [*Fejer and Scherliess*, 1997] and (2) the *AE* index is rather small while the ionospheric disturbance is very significant. The anomalous enhancement with increased outward perpendicular drift actually started from noon in the West Pacific Ocean area and became much more significant after sunset and continued into the next day morning as shown in Figures 2 and 5; so it is not consistent with the model of *Fejer and Scherliess* [1997] for the local time distribution of storm time dependence of equatorial dynamo zonal electric fields. The inconsistency can be attributable to the crude parameterization of the Joule heating at high latitudes and from the day-to-day variability of the quiet time atmospheric dynamo electric fields as pointed out by *Scherliess and Fejer* [1997]. Actually we used this model to calculate the disturbed drift during 26–28 June and found that the maximum equatorial upward drift does not exceed 1 m/s on 28 June. This is because the model explicitly depends on the previous 48 h of auroral *AE* index which is rather small for this case.

[22] Following the low-latitude electrodynamic theory [*Heelis et al.*, 1974], *Sastri* [1998] attributed the quiet time

abnormal postsunset increases in $h'F$ to the modifications of the equatorial thermospheric zonal winds and a flux tube-integrated Pedersen conductivity distribution favorable to a very effective F region dynamo; conditions which arose from an enhanced EIA process prior to postsunset. This creates a mechanism for the anomalous enhancement of TEC or N_mF_2 observed in the east Asian region but does not address the origin of the process. What causes the enhanced EIA process prior to the postsunset? A possible explanation for this intensified EIA may be due to the processes originating in the lower atmosphere. The processes which couple upward propagating tides, planetary waves and gravity waves with ionospheric changes occur, for instance, through modification of turbulent mixing and hence O/N_2 ratios, influences on E region conductivities, modulation of the temperature and wind structure of the thermosphere, and the generation of electric fields through the dynamo mechanism [*Forbes*, 1996]. Note that in the contour map of TEC in Figure 1, the postsunset EIA shows a wave structure during 26–29 June. The prereversal enhancement seems very weak on 27 and 29 June. The planetary-wave-type oscillation was observed in the mesospheric/lower thermospheric (MLT) winds observed at Wuhan station during summer 2002 using MF meteor radar [*Xiong et al.*, 2006]. From 4 to 24 June, the meridional winds from 82 to 100 km and ionospheric parameters $f$min, h_mF_2 and f_oF_2 displayed quasi-2-day wave oscillations. Unfortunately, there is a data gap for MLT wind data during the present case study. However, as *Mathews* [1998] pointed out, the prevailing periodicities in midlatitude sporadic E (E_s) result from the confluence of the vertical tidal wind shears in the lower thermosphere, particularly in the altitude range between 100 and 120 km. The planetary waves superimposed on tides may have its imprint in the E_s, which has been, for the first time, verified directly by *Haldoupis and Pancheva* [2002]. Using a series of ionosondes and MF radar in the east Asian region, *Igarashi and Kato* [2001] also demonstrated the possibility that planetary waves play a significant role in generating long-period oscillations in the formation of middle-latitude E_s.

[23] We are not very certain whether there were strong planetary waves during this period in the east Asian region. f_oE_s was, however, strong on local 26 and 28 June but weak on 25 and 27 June. We also checked the TIDI data within a 15-day window from 25 June to 10 July. There appears to be a region of enhanced 2.5-day wave with westward zonal wave number 3 between 30°N and 50°N in the meridional wind during 80–110 km (not shown here). Planetary waves in the neutral atmosphere cannot propagate directly upward to F_2-layer peak heights owing to the atmospheric viscosity and other factors. Model calculations do not predict significant penetration of planetary waves above 100–110 km [*Hagan et al.*, 1993]. However, upward propagating tides can modulate the E-layer dynamo electric fields and affect the F region. Recent simulations of the effect of upward propagating tidal energy in a global circulation model showed that several of the major diurnal tidal modes have a significant influence on the vertical plasma drifts in the F region during daytime while having practically no effect on the prereversal enhancement for conditions of high solar activity [*Millward et al.*, 2001]. This is due in part to the fact that the phase of the tidal forcing approaching zero at the terminators. Nevertheless, these model results show that the prereversal enhancement is clearly dependent upon the magnitude and phase of the semidiurnal tide during periods of low solar activity. Meanwhile, *Fesen* [1997] suggested that modulations of up to 20% in h_mF_2 and N_mF_2 during the daytime and as much as 40% during the night can be induced. Any modulation of the E region dynamo during the daytime is known to affect electron densities in the F region, and hence may alter the ratio of the integrated Pedersen conductivities in the two regions and, consequently, alter the strength of the prereversal enhancement. However, neither of the models in these studies was predicting variations as strong as we have reported here.

[24] A compromise candidate for the explanation for the anomalous enhancement would probably be the combination of the effects of auroral activity and tides. Note that at Wakkanai and Kokubunji, the enhancement started at 2000 UT on 27 June in Figure 2 and by the enhanced southward component of $V_{//}$ in Figure 5b, which suggests an increased meridional wind in the F region. Model simulations of *Lin et al.* [2005] assessed the relative contribution of the upward E × B drift and meridional winds in forming an extremely large enhancement of equatorial density crests. The upward electrodynamic drift lifts the plasma to higher altitudes which subsequently diffuses downward along magnetic field lines. If meridional winds blow equatorward at the same time the ion drag along magnetic field lines will oppose the downward diffusion and keep the plasma at altitudes where the recombination rate is lower. As a result, the peak density will increase significantly and the position of the peak will shift to higher latitudes.

5. Conclusion

[25] We present a case study of large ionospheric storm effects under geomagnetically quiet conditions using data in the Asian-Australian sector from 28 June 2002. Both GPS TEC and ionosonde show a continuous anomalous enhancement at low latitudes due to the enhanced fountain effect produced by large eastward electric fields. Moreover, this low-latitude anomalous enhancement was preceded by a positive storm effect of N_mF_2 at northern middle latitude, which could be caused by an enhanced equatorward wind due to the small auroral activities. The observation that large increases in f_oE_s occurred on the day prior to the start of anomalous enhancement suggest that the enhancement process originated with lower atmosphere processes and led to the extremely large day-to-day variability. Our result shows that in the summer hemisphere, the ionosphere was quite disturbed even though the geomagnetic activity was very low. Actually, both *Dst* and *Kp* indices indicated that June 2002 was rather quiet geomagnetically while the ionosphere in the Asian-Australian region was not quiet. This elicits another question: To what extent do the present geomagnetic indices reflect the real conditions of the disturbed ionosphere? The answer to this question is beyond the scope of this study.

[26] **Acknowledgments.** The *Ap* and *F*10.7 indices are downloaded from the NGDC database. Ionospheric data are provided from WDC for Ionosphere, Tokyo, National Institute of Information and Communications Technology, and Ionospheric Prediction Service of Australia. We express

special thanks to the Jet Propulsion Laboratory, California Institute of Technology, for offering GIM TEC. The ACE solar wind data are provided by CEDAR Data System from the Principal Investigator D. J. McComas of Southwest Research Institute. The hemispheric power index was provided by the NOAA Space Environment Center, Boulder, Colorado. This research was supported by National Natural Science Foundation of China (40725014) and National Important Basic Research Project (2006CB806306), and is also funded by the Knowledge Innovation Program of the Chinese Academy of Sciences.

[27] Zuyin Pu thanks Ivan Kutiev and another reviewer for their assistance in evaluating this paper.

References

Altadill, D., and E. M. Apostolov (2003), Time and scale size of planetary wave signatures in the ionospheric *F* region: Role of the geomagnetic activity and mesosphere/lower thermosphere winds, *J. Geophys. Res.*, *108*(A11), 1403, doi:10.1029/2003JA010015.

Altadill, D., E. M. Apostolov, J. Boška, J. Laštovička, and P. Săuli (2004), Planetary and gravity wave signatures in the *F* region ionosphere with impact to radio propagation predictions and variability, *Ann. Geophys.*, *47*(2/3), 1109–1119.

Behnke, R. A., and R. M. Harper (1973), Vector measurements of *F* region ion transport at Arecibo, *J. Geophys. Res.*, *78*, 8222–8234.

Bilitza, D. (2001), International Reference Ionosphere 2000, *Radio Sci.*, *36*, 261–275.

Blagoveshchensky, D. V., J. W. MacDougall, and A. V. Piatkova (2006), Ionospheric effects preceding the October 2003 Halloween storm, *J. Atmos. Sol. Terr. Phys.*, *68*, 821–831, doi:10.1016/j.jastp.2005.10.017.

Burešová, D., and J. Laštovička (2007), Pre-storm enhancements of foF2 above Europe, *Adv. Space Res.*, *39*(8), 1298–1303, doi:10.1016/j.asr.2007.03.003.

Burge, J. D., D. J. Eccles, W. King, and R. Rüster (1973), The effects of thermospheric winds on the ionosphere at low and middle latitudes during magnetic disturbances, *J. Atmos. Terr. Phys.*, *35*, 617–623, doi:10.1016/0021-9169(73)90192-X.

Burns, A. G., T. L. Killeen, W. Deng, G. R. Carignan, and R. G. Roble (1995), Geomagnetic storm effects in the low- to middle-latitude upper thermosphere, *J. Geophys. Res.*, *100*, 14,673–14,691.

Christensen, A. B., et al. (2003), Initial observations with the Global Ultraviolet Imager (GUVI) in the NASA TIMED satellite mission, *J. Geophys. Res.*, *108*(A12), 1451, doi:10.1029/2003JA009918.

Dabas, R. S., N. Sharma, M. G. K. Pillaia, and A. K. Gwal (2006), Day-to-day variability of equatorial and low latitude *F* region ionosphere in the Indian zone, *J. Atmos. Sol. Terr. Phys.*, *68*, 1269–1277, doi:10.1016/j.jastp.2006.03.009.

Danilov, A. D. (2001), F2-region response to geomagnetic disturbances, *J. Atmos. Sol. Terr. Phys.*, *63*, 441–449, doi:10.1016/S1364-6826(00)00175-9.

Depueva, A. K., A. V. Mikhailov, and V. K. Depuev (2005), Quiet time F2-layer disturbances at geomagnetic equator, *Int. J. Geomagn. Aeron.*, *5*, GI3001, doi:10.1029/2004GI000071.

Ezquer, R. G., et al. (2004), Day-to-day variability of ionospheric characteristics in the American sector, *Adv. Space Res.*, *34*, 1887–1893, doi:10.1016/j.asr.2004.03.016.

Fejer, B. G., and L. Scherliess (1995), Time dependent response of equatorial ionospheric electric field to magnetospheric disturbances, *Geophys. Res. Lett.*, *22*, 851–854.

Fejer, B. G., and L. Scherliess (1997), Empirical models of storm time equatorial zonal electric fields, *J. Geophys. Res.*, *102*(A11), 24,047–24,056.

Fesen, C. G. (1997), Theoretical effects of tides and auroral activity on the low-latitude ionosphere, *J. Atmos. Sol. Terr. Phys.*, *59*, 1521–1532, doi:10.1016/S1364-6826(96)00153-8.

Field, P. R., H. Rishbeth, R. J. Moffett, D. W. Idenden, T. J. Fuller-Rowell, G. H. Millward, and A. D. Aylward (1998), Modelling composition changes in F-layer storms, *J. Atmos. Sol. Terr. Phys.*, *60*, 523–543, doi:10.1016/S1364-6826(97)00074-6.

Forbes, J. M. (1996), Planetary waves in the thermosphere-ionic system, *J. Geomagn. Geoelectr.*, *48*, 91–98.

Forbes, J. M., S. E. Palo, and X. Zhang (2000), Variability of the ionosphere, *J. Atmos. Sol. Terr. Phys.*, *62*, 685–693, doi:10.1016/S1364-6826(00)00029-8.

Fuller-Rowell, T. J., M. Codrescu, and P. Wilkinson (2000), Quantitative modelling of the ionospheric response to geomagnetic activity, *Ann. Geophys.*, *18*, 766–781, doi:10.1007/s00585-000-0766-7.

Goncharenko, L., et al. (2006), Large variations in the thermosphere and ionosphere during minor geomagnetic disturbances in April 2002 and their association with IMF B_y, *J. Geophys. Res.*, *111*, A03303, doi:10.1029/2004JA010683.

Gonzalez, W. D., J. A. Joselyn, Y. Kamide, H. W. Kroehl, G. Rostoker, B. T. Tsurutani, and V. M. Vasyliunas (1994), What is a geomagnetic storm?, *J. Geophys. Res.*, *99*, 5771–5792.

Hagan, M. E., J. M. Forbes, and F. Vial (1993), A numerical investigation of the propagation of the quasi 2-day wave into the lower thermosphere, *J. Geophys. Res.*, *98*(D12), 23,193–23,205.

Haldoupis, C., and D. Pancheva (2002), Planetary waves and midlatitude sporadic E layers: Strong experimental evidence for a close relationship, *J. Geophys. Res.*, *107*(A6), 1078, doi:10.1029/2001JA000212.

Heelis, R. A., D. C. Kendall, R. J. Moffett, D. W. Windle, and H. Rishbeth (1974), Electric coupling of the *E*- and *F*-regions and its effects on *F*-region fields and winds, *Planet. Space Sci.*, *22*, 743–756, doi:10.1016/0032-0633(74)90144-5.

Ho, C. M., A. J. Mannucci, L. Sparks, X. Pi, U. J. Lindqwister, B. D. Wilson, B. A. Iijima, and M. J. Reyes (1998), Ionospheric total electron content perturbations monitored by the GPS global network during two northern hemisphere winter storms, *J. Geophys. Res.*, *103*, 26,409–26,420.

Huang, C.-M., A. D. Richmond, and M.-Q. Chen (2005), Theoretical effects of geomagnetic activity on low-latitude ionospheric electric field, *J. Geophys. Res.*, *110*, A05312, doi:10.1029/2004JA010994.

Huang, C.-S., J. C. Foster, and P. E. Erickson (2002), Effects of solar wind variations on the midlatitude ionosphere, *J. Geophys. Res.*, *107*(A8), 1192, doi:10.1029/2001JA009025.

Huang, X., and B. W. Reinisch (2001), Vertical electron content from ionograms in real time, *Radio Sci.*, *36*(2), 335–342.

Igarashi, K., and H. Kato (2001), The 2–16 day recurrence cycle of daily sporadic-*E* activity and its relation to planetary wave activity observed with MF radar in spring and summer 1996, *Adv. Space Res.*, *27*, 1271–1276, doi:10.1016/S0273-1177(01)00197-1.

Kane, R. P. (1973), Global evolution of F2-region storms, *J. Atmos. Terr. Phys.*, *35*, 1953–1966, doi:10.1016/0021-9169(73)90112-8.

Kazimirovsky, E., M. Herraiz, and B. A. De la Morena (2003), Effects on the ionosphere due to phenomena below it, *Surv. Geophys.*, *24*, 139–184, doi:10.1023/A:1023206426746.

Kouris, S. S., and D. N. Fotiadis (2002), Ionospheric variability: A comparative statistical study, *Adv. Space Res.*, *29*, 977–985, doi:10.1016/S0273-1177(02)00045-5.

Kutiev, I., Y. Otsuka, A. Saito, and S. Watanabe (2006), GPS observations of post-storm TEC enhancements at low latitudes, *Earth Planets Space*, *58*, 1479–1486.

Kutiev, I., Y. Otsuka, A. Saito, and S. Watanabe (2007), Low-latitude total electron content enhancement at low geomagnetic activity observed over Japan, *J. Geophys. Res.*, *112*, A07306, doi:10.1029/2007JA012385.

Laštovička, J. (2006), Forcing of the ionosphere by waves from below, *J. Atmos. Sol. Terr. Phys.*, *68*, 479–497, doi:10.1016/j.jastp.2005.01.018.

Laštovička, J., and P. Šauli (1999), Are planetary wave type oscillations in the F2 region caused by planetary wave modulation of upward propagating tides?, *Adv. Space Res.*, *24*, 1473–1476, doi:10.1016/S0273-1177(99)00708-5.

Lin, C. H., A. D. Richmond, R. A. Heelis, G. J. Bailey, G. Lu, J. Y. Liu, H. C. Yeh, and S.-Y. Su (2005), Theoretical study of the low- and midlatitude ionospheric electron density enhancement during the October 2003 superstorm: Relative importance of the neutral wind and the electric field, *J. Geophys. Res.*, *110*, A12312, doi:10.1029/2005JA011304.

Liu, L., W. Wan, M.-L. Zhang, B. Zhao, and B. Ning (2008), Prestorm enhancements in NmF2 and total electron content at low latitudes, *J. Geophys. Res.*, *113*, A02311, doi:10.1029/2007JA012832.

Lu, G., A. D. Richmond, R. G. Roble, and B. A. Emery (2001), Coexistence of ionospheric positive and negative storm phase under northern winter conditions: A case study, *J. Geophys. Res.*, *106*, 24,493–24,504.

Mannucci, A. J., B. D. Wilson, D. N. Yuan, C. H. Ho, U. J. Lindqwister, and T. F. Runge (1998), A global mapping technique for GPS-derived ionospheric total electron content measurements, *Radio Sci.*, *33*, 565–582.

Mathews, J. D. (1998), Sporadic E: Current views and recent progress, *J. Atmos. Sol. Terr. Phys.*, *60*, 413–435, doi:10.1016/S1364-6826(97)00043-6.

Mendillo, M. (2006), Storms in the ionosphere: Patterns and processes for total electron content, *Rev. Geophys.*, *44*, RG4001, doi:10.1029/2005RG000193.

Mikhailov, A. V., A. K. Depueva, and T. Y. Leschinskaya (2004), Morphology of quiet time F2-layer disturbances: High and lower latitudes, *Int. J. Geomagn. Aeron.*, *5*, GI006, doi:10.1029/2003GI000058.

Mikhailov, A. V., A. H. Depueva, and V. H. Depuev (2007a), Daytime F2-layer negative storm effect: What is the difference between storm-induced and Q-disturbance events?, *Ann. Geophys.*, *25*, 1531–1541.

Mikhailov, A. V., V. H. Depuev, and A. H. Depueva (2007b), Synchronous NmF2 and NmE daytime variations as a key to the mechanism of quiet-time F2-layer disturbances, *Ann. Geophys.*, *25*, 483–493.

Millward, G. H., et al. (2001), An investigation into the influence of tidal forcing on *F* region equatorial vertical ion drift using a global ionosphere-thermosphere model with coupled electrodynamics, *J. Geophys. Res.*, *106*, 24,733–24,744.

Paxton, L. J., et al. (2004), GUVI: A hyperspectral imager for geospace, in *Instruments*, *Science, and Methods for Geospace and Planetary Remote Sensing*, edited by C. A. Nardell et al., *Proc. SPIE Int. Soc. Opt. Eng.*, *5660*, 227–240.

Prölss, G. W. (1993), Common origin of positive ionospheric storms at middle latitudes and the geomagnetic activity effect at low latitudes, *J. Geophys. Res.*, *98*, 5981–5991.

Reinisch, B. W., X. Huang, I. A. Galkin, V. Paznukhov, and A. Kozlov (2005), Recent advances in real-time analysis of ionograms and ionospheric drift measurements with Digisondes, *J. Atmos. Sol. Terr. Phys.*, *67*, 1054–1062, doi:10.1016/j.jastp.2005.01.009.

Rishbeth, H. (2006), *F* region links with the lower atmosphere?, *J. Atmos. Sol. Terr. Phys.*, *68*, 469–478, doi:10.1016/j.jastp.2005.03.017.

Rishbeth, H., and M. Mendillo (2001), Patterns of F2-layer variability, *J. Atmos. Sol. Terr. Phys.*, *63*, 1661–1680, doi:10.1016/S1364-6826(01)00036-0.

Rishbeth, H., S. Ganguly, and J. C. G. Walker (1978), Field-aligned and field-perpendicular velocities in the ionospheric F2 layer, *J. Atmos. Terr. Phys.*, *40*, 767–784, doi:10.1016/0021-9169(78)90028-4.

Rishbeth, H., T. J. Fuller-Rowell, and D. Rees (1987), Diffusive equilibrium and vertical motion in the thermosphere during a severe magnetic storm: A computational study, *Planet. Space Sci.*, *35*, 1157–1165, doi:10.1016/0032-0633(87)90022-5.

Rüster, R., and J. W. King (1976), Negative ionospheric storms caused by thermospheric winds, *J. Atmos. Terr. Phys.*, *38*, 593–598, doi:10.1016/0021-9169(76)90153-7.

Sastri, J. H. (1998), On the development of abnormally large postsunset upward drift of equatorial *F* region under quiet geomagnetic conditions, *J. Geophys. Res.*, *103*(A3), 3983–3991.

Scherliess, L., and B. G. Fejer (1997), Storm time dependence of equatorial dynamo zonal electric fields, *J. Geophys. Res.*, *102*(A11), 24,037–24,046.

Strickland, D. J., R. R. Meier, R. L. Walterscheid, J. D. Craven, A. B. Christensen, L. J. Paxton, D. Morrison, and G. Crowley (2004), Quiet-time seasonal behavior of the thermosphere seen in the far ultraviolet dayglow, *J. Geophys. Res.*, *109*, A01302, doi:10.1029/2003JA010220.

Su, S.-Y., H. C. Yeh, C. K. Chao, and R. A. Heelis (2002), Observation of a larger density dropout across the magnetic field at about 600 km during the 6–7 April 2000 magnetic storm, *J. Geophys. Res.*, *107*(A11), 1404, doi:10.1029/2001JA007552.

Xiong, J., W. Wan, B. Ning, L. Liu, and Y. Gao (2006), Planetary wave-type oscillations in the ionosphere and their relationship to mesospheric/lower thermospheric and geomagnetic disturbances at Wuhan (30.61N, 114.51E), *J. Atmos. Sol. Terr. Phys.*, *68*, 498–508, doi:10.1016/j.jastp.2005.03.018.

Zhang, M. L., J. K. Shi, X. Wang, and S. M. Radicella (2004), Ionospheric variability at low latitude station: Hainan, China, *Adv. Space Res.*, *34*, 1860–1868, doi:10.1016/j.asr.2004.04.005.

Zhao, B., W. Wan, and L. Liu (2005), Response of equatorial anomaly to the October-November 2003 superstorm, *Ann. Geophys.*, *23*, 693–706.

K. Igarashi and M. Nakamura, National Institute of Information and Communications Technology, Tokyo 184-8795, Japan.

G. Li, L. Liu, Z. Ren, W. Wan, and B. Zhao, Beijing National Observatory of Space Environment, Institute of Geology and Geophysics, Chinese Academy of Sciences, Beijing 100029, China. (zbqjz@mail.igcas.ac.cn)

L. J. Paxton, Johns Hopkins University Applied Physics Laboratory, Laurel, MD 20723, USA.

S.-Y. Su, Institute of Space Science and Center for Space and Remote Sensing Research, National Central University, Chung-Li 32054, Taiwan. (sysu@jupiter.ss.ncu.edu.tw)